# Dalton Transactions

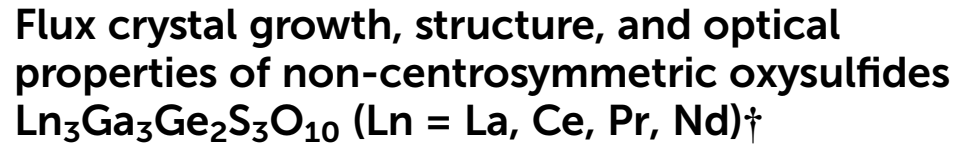


**PAPER** 

View Article Online
View Journal | View Issue



**Cite this:** *Dalton Trans.*, 2025, **54**, 10433



Hong Yan, a,b Kotaro Fujii, c,d Yoshitaka Matsushita, b e Masatomo Yashima, b c Kazunari Yamaura and Yoshihiro Tsujimoto k \*a,b

Received 9th May 2025, Accepted 4th June 2025 DOI: 10.1039/d5dt01100k

rsc.li/dalton

### Introduction

Metal oxychalcogenides, in which oxide and chalcogenide ions coexist in one structure, have provided a playground for solid-state scientists to explore fascinating properties because of the large differences in their ionic radii, electronegativities, oxidation states, and polarizabilities. One recent significant advantage of oxychalcogenide compounds is the design of nonlinear optical (NLO) materials. Stabilizing metal-centered heteroleptic coordination environments containing both oxide and chalcogenide ligands offers a chance to significantly increase the optical band gaps and second harmonic generation (SHG) responses compared with chalcogenides, because

Single-crystal X-ray diffraction (SCXRD) analyses of  $La_3Ga_3Ge_2S_3O_{10}$ ,  $La_3Ga_3Si_2S_3O_{10}$ , and  $Nd_3Ga_3Ge_2S_3O_{10}$  have demonstrated that they are isostructural and adopt a hexagonal unit cell in the space group  $P\bar{6}2c.^{8,12,13}$  However, they exhibited different atomic distribution patterns, as described below. In the

of the presence of O 2p orbitals in the valence band maximum and acentric polyhedral units with polar atomic displacement. Since the discovery of the first phase-matchable oxyselenide BaGeOSe<sub>2</sub> and oxysulfide SrZn<sub>2</sub>S<sub>2</sub>O with strong SHG intensities,5,6 a number of new oxychalcogenides have been reported to show good balanced properties with high SHG responses, high laser damage thresholds, and wide optical band gaps.<sup>3,7</sup> While most of the reported NLO oxychalcogenide compounds were focused on applications in the infrared region because of their relatively small band gap values (<4 eV), a new oxysulfide La<sub>3</sub>Ga<sub>3</sub>Ge<sub>2</sub>S<sub>3</sub>O<sub>10</sub> consisting of (Ga/Ge)O<sub>4</sub> and (Ga/Ge)S2O2 tetrahedra exhibited promising properties for applications in the UV regions (Fig. 1): the exceptionally large band gap value (4.70 eV), short cutoff edge (250 nm), and strong SHG response twice that of the KH2PO4 benchmark compound.8 The fundamental origin of the large bandgap and strong SHG response can be attributed to the lack of an allsulfide coordination environment and the presence of a heteroleptic coordination environment, 9,10 as in [Ba<sub>2</sub>F<sub>2</sub>][Ge<sub>2</sub>O<sub>3</sub>S<sub>2</sub>]  $(1.4 \times AgGaS_2)$ , <sup>11</sup>  $Nd_3Ga_3Ge_2S_3O_{10}$   $(1.7 \times KDP, 0.8 \times AgGaS_2)$ , <sup>12</sup> and  $La_3Ga_3Si_2S_3O_{10}$  (1.7 × KDP, 0.3 × AgGaS<sub>2</sub>).<sup>13</sup>

<sup>&</sup>lt;sup>a</sup>Research Center for Materials Nanoarchitechtonics (MANA), National Institute for Materials Science (NIMS), 1-1 Namiki, Tsukuba, Ibaraki 305-0044, Japan. E-mail: TSUJIMOTO. Yoshihiro@nims.go.jp

<sup>&</sup>lt;sup>b</sup>Graduate School of Chemical Sciences and Engineering, Hokkaido University, North 10 West 8, Kita-ku, Sapporo, Hokkaido 060-0810, Japan

<sup>&</sup>lt;sup>c</sup>Department of Chemistry, School of Science, Institute of Science Tokyo, 2-12-1-W4-17, Ookayama Meguro-ku, Tokyo, 152-8551, Japan

<sup>&</sup>lt;sup>d</sup>Faculty of Bioscience and Applied Chemistry, Department of Chemical Science and Technology, Hosei University, 3-5-4 Kajino-cho, Koganei, Tokyo 184-8584, Japan <sup>e</sup>Materials Analysis Station, NIMS, 1-2-1 Sengen, Tsukuba, Ibaraki 305-0047, Japan † Electronic supplementary information (ESI) available. CCDC 2449159, 2449160, 2449238 and 2449239. For ESI and crystallographic data in CIF or other electronic format see DOI: https://doi.org/10.1039/d5dt01100k

Paper Dalton Transactions

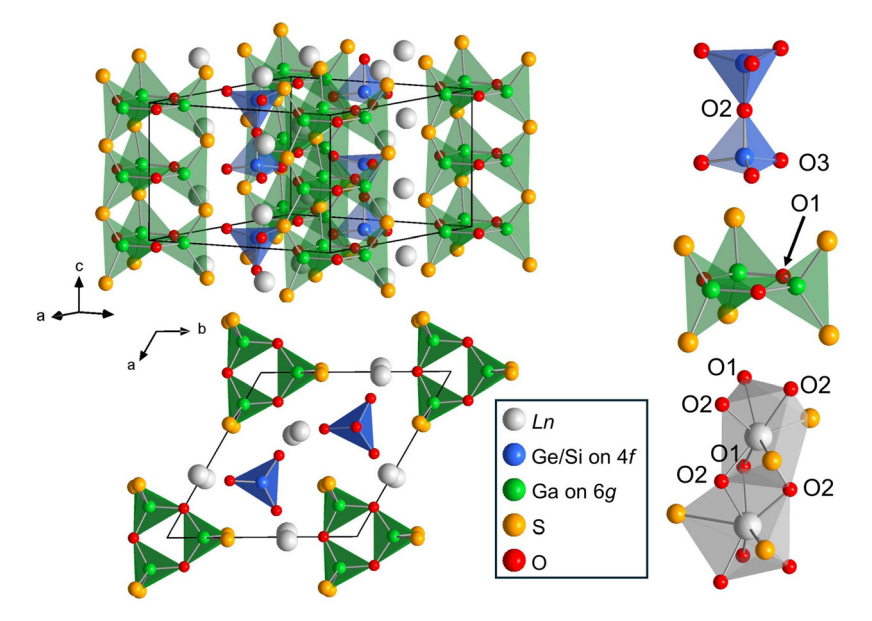


Fig. 1 Side and top views of the crystal structure of  $Ln_3Ga_3Ge_2S_3O_{10}$  (Ln = La, Ce, Pr, Nd), which possesses one-dimensional chains of  $LnS_2O_6$  square antiprisms, and isolated dimers and triangular tubes composed of M1O<sub>4</sub> tetrahedra and M2S<sub>2</sub>O<sub>2</sub> tetrahedra, respectively.

latter two phases, the Ga and Ge/Si atoms were located on Wyckoff positions 6g and 4f, respectively, to take the GaS<sub>2</sub>O<sub>4</sub> and (Ge/Si)O<sub>4</sub> tetrahedral geometries (Fig. 1). These tetrahedra formed <sup>1</sup>/<sub>∞</sub>[Ga<sub>3</sub>S<sub>3</sub>O<sub>3</sub>] triangular tubes and (Ge/Si)<sub>2</sub>O<sub>7</sub> tetrahedral dimers, which were separated by (La/Nd)S2O6 square antiprisms in the ab plane. In contrast, La<sub>3</sub>Ga<sub>3</sub>Ge<sub>2</sub>S<sub>3</sub>O<sub>10</sub> exhibited a random distribution of Ga and Ge over the 6g and 4f sites at an atomic ratio of 3:2. It is reasonable for Si ions to adopt an all-oxygen homoleptic coordination geometry because they rarely form heteroleptic coordination polyhedra, while the difference in cation ordering patterns in La<sub>3</sub>Ga<sub>3</sub>Ge<sub>2</sub>S<sub>3</sub>O<sub>10</sub> and Nd<sub>3</sub>Ga<sub>3</sub>Ge<sub>2</sub>S<sub>3</sub>O<sub>10</sub> is non-trivial. In previous studies, the bond-valence-sum (BVS) values for Ga/Ge on 6g and 4f were estimated to be 3.04 and 3.92, respectively. This implied a Ga/Ge ordered state as in the Nd analog, although structural refinements based on the cationordered model were unstable. In oxides containing both Ga and Ge atoms, the identification of the distribution of these cations by XRD analysis is of major concern because of their similar X-ray scattering factors. 14-16

In this study, we reexamined the Ga/Ge cation disordered state of  $La_3Ga_3Ge_2S_3O_{10}$  and newly synthesized a series of  $Ln_3Ga_3Ge_2S_3O_{10}$  (Ln = La, Ce, Pr, Nd) by both molten chloride flux methods and conventional solid-state reactions. Neutron powder diffraction (NPD), in addition to SCXRD, was employed to characterize the crystal structure, especially the Ga/Ge cation ordered pattern.

# Experimental section

#### Reagents

 $La_2S_3$  (Kojundo Chemical Laboratory, 3 N),  $La_2O_3$  (Rare Metallic, 4 N),  $CeO_2$  (Rare Metallic, 4 N),  $Pr_6O_{11}$  (Rare Metallic,

#### Crystal growth and elemental analysis

Single crystals of Ln<sub>3</sub>Ga<sub>3</sub>Ge<sub>2</sub>S<sub>3</sub>O<sub>10</sub> (Ln = La, Ce, Pr, Nd) were obtained by the flux growth method using a BaCl<sub>2</sub>-NaCl eutectic molten salt. For Ln = La, La<sub>2</sub>S<sub>3</sub> (0.5 mmol), Ga<sub>2</sub>O<sub>3</sub> (0.5 mmol), and GeO<sub>2</sub> (0.5 mmol) were combined according to the literature.8 For Ln = Ce and Pr, CeO<sub>2</sub> (0.6 mmol)/Pr<sub>6</sub>O<sub>11</sub> (0.1 mmol), Ga<sub>2</sub>O<sub>3</sub> (0.3 mmol), Ge (0.4 mmol), and S (0.6 mmol) were combined. For Ln = Nd,  $Nd_2O_3$  (0.3 mmol), Ga<sub>2</sub>O<sub>3</sub> (0.3 mmol), Ge (0.3 mmol), S (0.6 mmol) and GeO<sub>2</sub> (0.1 mmol) were combined. Each set of starting materials was loaded in an alumina crucible with BaCl<sub>2</sub> (2.7 mmol) and NaCl (4.0 mmol). The crucibles were flame-sealed in fused silica tubes under a vacuum of 1 Pa, heated in a muffle furnace to 850 °C at 5 °C min<sup>-1</sup>, held at this temperature for 24 h, cooled to 550 °C at 0.08 °C min<sup>-1</sup>, and finally cooled naturally to room temperature. The products were then washed with sonicated water and extracted from the flux. Transparent rodshaped crystals of the title compounds were collected by vacuum filtration with approximately yields of 65% for La, 10% for Ce, 30% for Pr, and 60% for Nd based on lanthanide 2). Elemental analysis of single

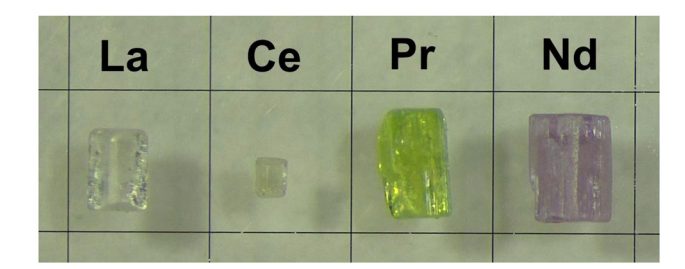


Fig. 2 Photographs of single crystals of  $Ln_3Ga_3Ge_2S_3O_{10}$  (Ln = La, Ce, Pr, Nd) on a 1 mm-grid glass plate.

 ${\rm Ln_3Ga_3Ge_2S_3O_{10}}$  was performed using a scanning electron microscope (SEM, HITACHI, S-43000) equipped with an energy dispersive X-ray (EDX) spectrometer. The accelerating voltage was set to 15 keV. EDX analysis indicated a  ${\rm Ln:Ga:Ge:S}$  atomic ratio of approximately 3:3:2:3, which was in good agreement with the chemical composition determined by single-crystal structure analysis.

#### Solid state reaction

Polycrystalline powder samples of Ln<sub>3</sub>Ga<sub>3</sub>Ge<sub>2</sub>S<sub>3</sub>O<sub>10</sub> (Ln = La-Nd) were synthesized by conventional solid-state reactions. The Ln = La, Pr, and Nd phases were synthesized from a stoichiometric mixture of La<sub>2</sub>O<sub>3</sub> (0.3 mmol), Ga<sub>2</sub>O<sub>3</sub> (0.3 mmol),  $GeO_2$  (0.1 mmol), Ge (0.3 mmol), and S (0.6 mmol) for Ln =La, Pr<sub>6</sub>O<sub>11</sub> (0.1 mmol), Ga<sub>2</sub>O<sub>3</sub> (0.3 mmol), Ge (0.4 mmol) and S (0.6 mmol) for Ln = Pr, Nd<sub>2</sub>O<sub>3</sub> (0.3 mmol), Ga<sub>2</sub>O<sub>3</sub> (0.3 mmol),  $GeO_2$  (0.1 mmol), Ge (0.3 mmol), and S (0.6 mmol) for Ln =Nd. The Ln = Ce phase was synthesized using a mixture of CeO<sub>2</sub> (0.6 mmol), Ga<sub>2</sub>O<sub>3</sub> (0.3 mmol), Ge (0.4 mmol), and S (0.6 mmol), which contains 0.1 mmol excess of oxygen compared with the stoichiometry of Ce<sub>3</sub>Ga<sub>3</sub>Ge<sub>2</sub>S<sub>3</sub>O<sub>10</sub>. Each set of starting materials was ground with an agate mortar and pestle, pressed into a pellet, sealed in a silica tube under a vacuum of 1 Pa, and heated in a muffle furnace at 1000 °C for 24 h. For neutron powder diffraction studies, scaled-up syntheses (approximately 10 times the amount) of polycrystalline powder samples of La<sub>3</sub>Ga<sub>3</sub>Ge<sub>2</sub>S<sub>3</sub>O<sub>10</sub> and Nd<sub>3</sub>Ga<sub>3</sub>Ge<sub>2</sub>S<sub>3</sub>O<sub>10</sub> were performed using a similar synthesis procedure.<sup>8,12</sup>

## Single crystal structure determination

X-ray intensity data of single crystals of  $\rm Ln_3Ga_3Ge_2S_3O_{10}$  (Ln = La–Nd) were collected using a Rigaku XtaLAB mini II diffractometer (Mo Kα radiation). Data collection covered more than 96% of the reciprocal space to  $2\theta_{\rm max} \sim 60^{\circ}$  with  $R_{\rm int} = 4.17\%$  for La, 3.42% for Ce, 3.19% for Pr, and 3.31% for Nd after absorption correction. The crystal structure was solved using a dual-space algorithm method (SHELXT)<sup>17</sup> and refined using a full-matrix least-squares method with SHELXL<sup>18</sup> using an Olex2<sup>19</sup> graphical user interface.

#### Powder XRD and UV-Vis-NIR

Powder XRD patterns were collected on a Rigaku MiniFlex-600 diffractometer (Cu K $\alpha$  radiation) from the  $2\theta$  range of 5–70°

with a step of 0.02° at room temperature. The UV-vis-NIR reflectance spectra were collected using a Shimadzu UV- 2600 UV-Vis-NIR spectrometer (used in the diffuse reflectance mode) equipped with an integrating sphere in the range of 220–1200 nm. Deuterium and halogen lamps were used as sources of UV and visible-NIR light, respectively. The recorded reflectance spectra were converted into the absorption data *via* the Kubelka-Munk function.

#### Powder neutron diffraction

Time-of-flight neutron powder diffraction (NPD) measurements were conducted at room temperature using an iMATERIA $^{20}$  installed at J-PARC MLF BL20 in Japan. La $_3$ Ga $_3$ Ge $_2$ S $_3$ O $_{10}$  (2.44 g) and Nd $_3$ Ga $_3$ Ge $_2$ S $_3$ O $_{10}$  (2.57 g) were independently loaded into a vanadium can with 5.8 mm inner diameter, and the diffraction data were collected using a back-scattering detector bank. The NPD data were analyzed by Rietveld refinement using the Z-code program. $^{21}$ 

## Results and discussion

# Structure determination using single-crystal X-ray diffraction data

Typical dimensions of single crystals of Ln<sub>3</sub>Ga<sub>3</sub>Ge<sub>2</sub>S<sub>3</sub>O<sub>10</sub> (Ln = La-Nd) were ranged from  $0.1 \times 0.1 \times 0.2$  to  $0.5 \times 0.5 \times 0.8$  mm<sup>3</sup>, indicating that these crystals grew preferentially along the c-axis. Single crystals of La<sub>3</sub>Ga<sub>3</sub>Ge<sub>2</sub>S<sub>3</sub>O<sub>10</sub> and Nd<sub>3</sub>Ga<sub>3</sub>Ge<sub>2</sub>S<sub>3</sub>O<sub>10</sub> were colorless and pale purple, respectively, as previously reported (Fig. 2). Ce<sub>3</sub>Ga<sub>3</sub>Ge<sub>2</sub>S<sub>3</sub>O<sub>10</sub> and Pr<sub>3</sub>Ga<sub>3</sub>Ge<sub>2</sub>S<sub>3</sub>O<sub>10</sub> were colorless and lime-green, respectively. The colors of Pr<sub>3</sub>Ga<sub>3</sub>Ge<sub>2</sub>S<sub>3</sub>O<sub>10</sub> and Nd<sub>3</sub>Ga<sub>3</sub>Ge<sub>2</sub>S<sub>3</sub>O<sub>10</sub> are characteristic of f-f transitions in Pr3+ and Nd3+. These single crystals are stable in air and water insoluble. Single-crystal structure analysis of  $Ln_3Ga_3Ge_2S_3O_{10}$  (Ln = La-Nd) was performed at room temperature. As reported previously, the Ln = La phase adopts the hexagonal space group  $P\bar{6}2c$  (no. 190) with lattice parameters of a = 10.1701(4) Å and c = 7.5198(3) Å. Additionally, the structure refinement based on the cation ordered model that Ga and Ge atom occupied 6g and 4f sites, respectively, smoothly converged in contrast to our previous report. The Ln = Ce-Nd analogs were also found to adopt the same space group with lattice parameters, which were proportional to the ionic radius of Ln<sup>3+</sup> ions (Fig. 3). The structure refinements indicated the Ga/Ge ordering, as reported previously for Nd<sub>3</sub>Ga<sub>3</sub>Ge<sub>2</sub>S<sub>3</sub>O<sub>10</sub>. <sup>12</sup> The details of the final refined structure for all the phases are listed in Table 1. The atomic coordinates and isotropic thermal displacement parameters are listed in Table 2 and the anisotropic displacement parameters are listed in Table S1.† Selected interatomic distances and angles are listed in Table S2.† The metal-ligand bond distances in GeO4 and GaS2O2 tetrahedra in all phases are very close to the sum of their ionic radii ( $r_{\text{Ge}^{4+}} = 0.39 \text{ Å}, r_{\text{Ga}^{3+}} = 0.47 \text{ Å}, r_{\text{O}^{2-}} = 1.4 \text{ Å}, r_{\text{S}^{2-}} =$ 1.84 Å).<sup>22</sup> In contrast, in the LnS<sub>2</sub>O<sub>6</sub> tetrahedron, the Ln–O/Ln– S bond distances are broad compared to the sum of their ionic radii, but their average bond distances are in good agreement

Paper Dalton Transactions

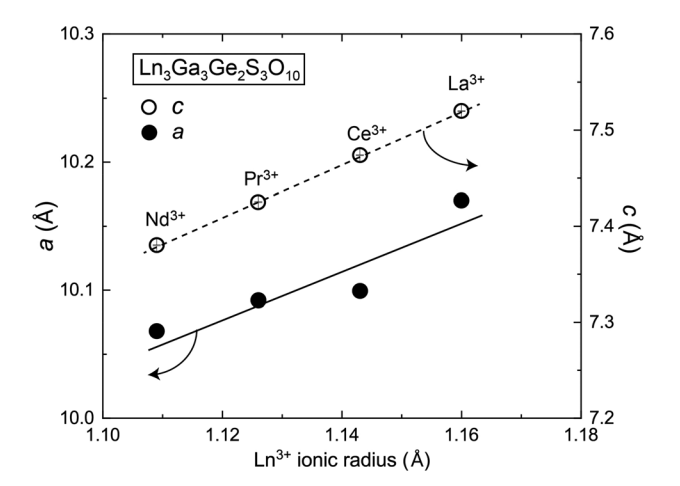


Fig. 3 The a-axis and c-axis lengths plotted as a function of the ionic radius of  $Ln^{3+}$ .

with the sum of their ionic radii. Bond valence sum (BVS) calculations<sup>23</sup> were carried out for all the atoms, as shown in Table 3. The BVS values of Ln (= La, Ce, Pr, Nd), Ga, and Ge atoms were consistent with the nominal oxidation number expected from the chemical composition.

#### X-ray powder diffraction

Fig. 4 shows the room-temperature X-ray powder diffraction patterns of polycrystalline  $\rm Ln_3Ga_3Ge_2S_3O_{10}$  (Ln = La–Nd) samples synthesized by conventional high-temperature solid-state reactions. These compounds were obtained in nearly a single phase. All of these XRD patterns could be readily indexed to the hexagonal cell in the space group  $P\bar{6}2c$ , except for a few minor peaks that could be assigned to  $\rm GeO_2$ . Similar to the single-crystal structure analysis, the lattice constants of

the polycrystalline samples also varied with the ionic radius of Ln<sup>3+</sup> (Fig. S1†).

# Structure determination using neutron powder diffraction data

To investigate the Ga and Ge atom distribution in La<sub>3</sub>Ga<sub>3</sub>Ge<sub>2</sub>S<sub>3</sub>O<sub>10</sub>, neutron powder diffraction experiments were performed on La<sub>3</sub>Ga<sub>3</sub>Ge<sub>2</sub>S<sub>3</sub>O<sub>10</sub> at room temperature, together with Nd<sub>3</sub>Ga<sub>3</sub>Ge<sub>2</sub>S<sub>3</sub>O<sub>10</sub>, for comparison. Fig. 5 shows the results of Rietveld refinements of these two oxysulfides. For both La<sub>3</sub>Ga<sub>3</sub>Ge<sub>2</sub>S<sub>3</sub>O<sub>10</sub> and Nd<sub>3</sub>Ga<sub>3</sub>Ge<sub>2</sub>S<sub>3</sub>O<sub>10</sub>, the profile fitting to the Ga/Ge ordered model smoothly converged well with reliable factors,  $R_{\rm wp} = 5.40$ ,  $R_{\rm p} = 4.24$ ,  $R_{\rm B} = 2.58$  for La and  $R_{\rm wp} = 8.24$ ,  $R_{\rm p} = 5.79$ ,  $R_{\rm B} = 5.97$  for Nd (Fig. 5). To examine the possibility of Ga/Ge atoms being disordered, structure refinement was performed under the assumption that Ga and Ge atoms are disordered at the 6g and 4f sites. The results showed that 6g and 4f sites were more than 99% occupied by Ga and Ge atoms, respectively, within statistical errors. Thus, we conclude that the Ga and Ge atoms in the polycrystalline samples are ordered like the single crystals. Tables S3 and Table 3 summarize the final obtained crystallographic data including isotropic displacement parameters for all atoms. The occupancy factors of Ga on 6g and Ge on 4f were fixed at unity in the final refinement.

# Ga/Ge cation ordering and size effect of Ln3+ on the lattices

The present structure refinements against the SCXRD and NPD data of  $La_3Ga_3Ge_2S_3O_{10}$  revealed the Ga/Ge cation order, which differed from the Ga/Ge disorder characterized in the previous study.<sup>8</sup> One possible reason for the cation disordering can be ascribed to a technical problem in the structure refinements. We reviewed the previous SCXRD data from the beginning and found that the cation ordered state was also stabil-

Table 1 Results of structure refinement of Ln<sub>3</sub>Ga<sub>3</sub>Ge<sub>2</sub>S<sub>3</sub>O<sub>10</sub> (Ln = La, Ce, Pr, Nd) using single-crystal XRD data

Formula	$La_3Ga_3Ge_2S_3O_{10}$	$Ce_3Ga_3Ge_2S_3O_{10}$	$Pr_3Ga_3Ge_2S_3O_{10}$	Nd <sub>3</sub> Ga <sub>3</sub> Ge <sub>2</sub> S <sub>3</sub> O <sub>10</sub>
Formula weight	1027.25	1030.88	1033.25	1043.24
T(K)	297	297	293	294
Crystal system	Hexagonal	Hexagonal	Hexagonal	Hexagonal
Space group	$P\bar{6}2c$	$P\bar{6}2c$	$P\bar{6}2c$	$P\bar{6}2c$
a (Å)	10.1701(4)	10.0993(4)	10.0921(7)	10.0682(5)
$c(\mathring{A})$	7.5198(3)	7.4738(4)	$7.4251(5)^{2}$	7.3802(5)
$\alpha (\circ)$	90	90	90	90
$\beta$ (°)	90	90	90	90
γ (°)	120	120	120	120
$V(\mathring{\mathbf{A}}^3)$	673.58(6)	660.17(6)	654.93(9)	647.89(8)
Z	2	2	2	2
$ ho_{ m calc}  ({ m g \ cm}^{-3})$	5.065	5.186	5.240	5.348
$\mu  (\mathrm{mm}^{-1})$	20.096	21.201	22.042	23.023
$F_{000}$	912	918	924	930
$\theta$ (°)	3.534-30.53	2.329-30.64	3.5840-30.38	2.336-30.607
R <sub>int</sub> (%)	4.17	3.42	3.19	3.31
No. of reflections (collected/unique)	9330/734	9529/723	2246/467	2524/658
Goodness of fit on $F^2$	1.061	1.083	0.977	1.041
$R_1$ , w $R_2$ $[I > 2\sigma(I)]$	0.0109, 0.0251	0.0109/0.0208	0.0128/0.0234	0.0192/0.0378
$R_1$ , w $R_2$ (all data)	0.0114, 0.0252	0.0126/0.0210	0.0136/0.0236	0.0216/0.0386
Diff peak, hole (e Å <sup>-3</sup> )	0.433, -0.387	0.454, -0.494	0.373, -0.330	0.712, -0.644
Flack parameter	-0.002(13)	0.001(12)	-0.03(3)	-0.05(3)

Table 2 Crystallographic and refinement data obtained from single-crystal structure analysis of Ln<sub>3</sub>Ga<sub>3</sub>Ge<sub>2</sub>S<sub>3</sub>O<sub>10</sub> (Ln = La, Ce, Pr, Nd)

Atom	Site	x	у	z	Occupancy	$U_{ m iso}$ / ${ m \AA}^2$
La <sub>3</sub> Ga <sub>3</sub> Ge <sub>2</sub> S <sub>3</sub>	3O <sub>10</sub>					
La	6h	0.35751(3)	0.38034(3)	1/4	1	0.00771(8)
Ge	4f	2/3	1/3	0.51367(7)	1	$0.00446(13)^{a}$
Ga	6 <i>g</i>	0	0.18935(5)	0	1	$0.00652(12)^{a}$
S	6h	0.01248(14)	0.32093(14)	1/4	1	0.0106(2)
O1	6 <i>g</i>	0.1757(3)	0.1757(2)	0	1	0.0089(7)
O2	12i	0.5052(3)	0.3439(3)	0.4667(3)	1	0.0111(5)
O3	2c	2/3	1/3	3/4	1	0.033(2)
Ce <sub>3</sub> Ga <sub>3</sub> Ge <sub>2</sub> S	$_{3}O_{10}$					
Ce	6h	0.35730(3)	0.38047(3)	1/4	1	0.00888(7)
Ge	4f	2/3	1/3	0.51309(7)	1	0.00542(13)
Ga	6 <i>g</i>	0	0.19034(6)	0	1	0.00761(11)
S	6h	0.01396(15)	0.32373(15)	1/4	1	0.0120(3)
O1	6 <i>g</i>	0.1770(3)	0.1770(3)	0	1	0.0111(7)
O2	12i	0.5038(3)	0.3439(3)	0.4663(3)	1	0.0115(5)
O3	2c	2/3	1/3	3/4	1	0.032(2)
Pr <sub>3</sub> Ga <sub>3</sub> Ge <sub>2</sub> S <sub>3</sub>	$O_{10}$					
Pr	6h	0.35754(5)	0.38139(6)	1/4	1	0.00797(13)
Ge	4f	2/3	1/3	0.51145(11)	1	0.0039(2)
Ga	6 <i>g</i>	0	0.19057(10)	0	1	0.0070(2)
S	6h	0.01632(2)	0.3260(2)	1/4	1	0.0118(5)
O1	6 <i>g</i>	0.1764(6)	0.1764(6)	0	1	0.0135(15)
O2	12i	0.5033(4)	0.3433(4)	0.4658(5)	1	0.0106(9)
O3	2c	2/3	1/3	1/4	1	0.036(4)
Nd <sub>3</sub> Ga <sub>3</sub> Ge <sub>2</sub> S	$_{3}O_{10}$					
Nd	6 <i>h</i>	0.35688(5)	0.38212(6)	1/4	1	0.00923(14)
Ge	4f	2/3	1/3	0.51014(13)	1	0.0056(2)
Ga	6 <i>g</i>	0	0.19121(11)	0	1	0.0076(2)
S	6h	0.0183(3)	0.3287(3)	1/4	1	0.0121(5)
O1	6 <i>g</i>	0.1778(6)	0.1778(6)	0	1	0.0123(14)
O2	12 <i>i</i>	0.5029(5)	0.3435(5)	0.4643(6)	1	0.0114(9)
O3	2c	2/3	1/3	1/4	1	0.036(4)

Table 3 The values of bond-valence-sum calculations for Ln, Ge, and Ga sites obtained from the single crystal structure analysis

Formula	Ln at 6h	Ga at 6g	Ge at 4f
La <sub>3</sub> Ga <sub>3</sub> Ge <sub>2</sub> S <sub>3</sub> O <sub>10</sub>	2.81	3.03	3.91
$Ce_3Ga_3Ge_2S_3O_{10}$	2.83	2.95	4.03
$Pr_3Ga_3Ge_2S_3O_{10}$	2.92	2.98	4.05
$Nd_3Ga_3Ge_2S_3O_{10}$	2.81	2.98	4.04

ized. Perhaps, due to similar X-ray scattering factors of Ga and Ge atoms, the previous refinements fell into a local minimum that stabilizes the cation disordered state.

As shown in Fig. 3, the lattice parameters change linearly with the ionic radius of the Ln3+. On the other hand, the distortion index24 (D) around the metal centers, which was calculated using the metal-anion bond distances determined from the SCXRD data, exhibits unusual behaviors against the size of  $Ln^{3+}$  (Table S4†). The D values for the Ge-centered tetrahedra in Ln = La are 0.00911, which are remarkably larger than those for the corresponding tetrahedra in the other Ln ions by 15-31%, while the D values for the Ln- and Ga-centered polyhedra remained similar regardless of the Ln species. This can be rationalized by considering the volume of LnO<sub>6</sub>S<sub>2</sub> square antiprisms, which form three-member rings via common S atoms in the ab plane and surround the Ga/Ge-centered tetrahedra. The GeO<sub>4</sub> tetrahedron may be too small to fit into a framework consisting of LaS2O6, which has the largest volume compared to other Ln-centered polyhedra. We attempted to synthesize other members with Ln3+ smaller than Nd3+, but it was not successful.

#### Optical properties and bandgap

Fig. 6a shows the UV-Vis-NIR diffuse reflectance of  $Ln_3Ga_3Ge_2S_3O_{10}$  (Ln = La-Nd). The spectra of Ln = Pr and Nd exhibited a UV cutoff edge close to 250 nm, as seen for La<sub>3</sub>Ga<sub>3</sub>Ge<sub>2</sub>S<sub>3</sub>O<sub>10</sub>, which can be attributed to an optical transition from the valence band maximum composed of Ln-5d and Ga-4s, 4p orbitals to the conduction band minimum composed of O-2p and S-3p orbitals.<sup>8,12</sup> A series of complex optical bands in a broad range of wavelengths result from the f-f transitions characteristic of the localized 4f orbitals of Ln ions. In contrast, the Ln = Ce phase exhibited stepwise absorption below 430 nm, followed by a cutoff edge at 340 nm. This characteristic absorption is due to the presence of the Ce-4f ground state between the VBM and CBM: optical transitions from the Ce-4f ground state to the lowest and second lowest Ce-4d states occur. Fig. 6b shows the absorption spectra converted from the diffuse reflectance spectra using the Kubelka-

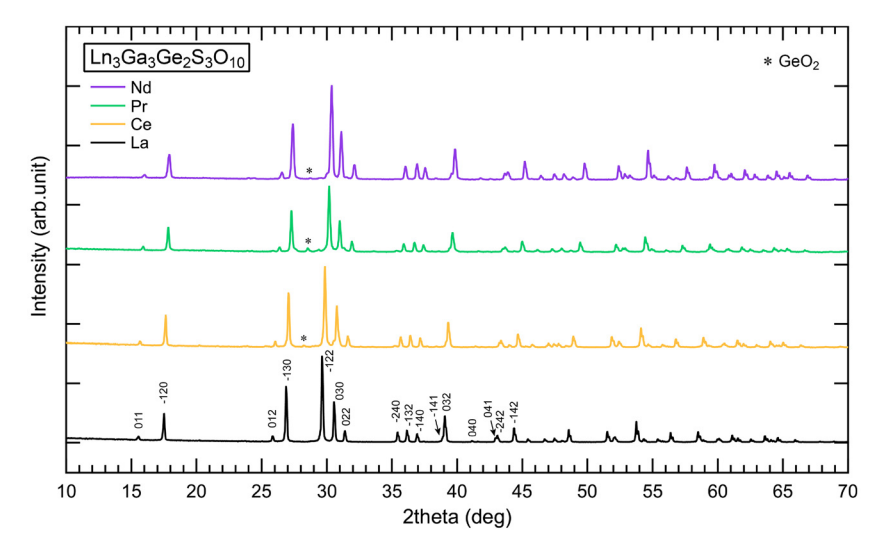


Fig. 4 Room-temperature X-ray powder diffraction patterns of  $Ln_3Ga_3Ge_2S_3O_{10}$  (Ln = La, Ce, Pr, Nd) polycrystalline samples obtained *via* high-temperature solid-state reactions. All phases can be assigned to a hexagonal cell in the space group  $P\bar{6}2c$ .

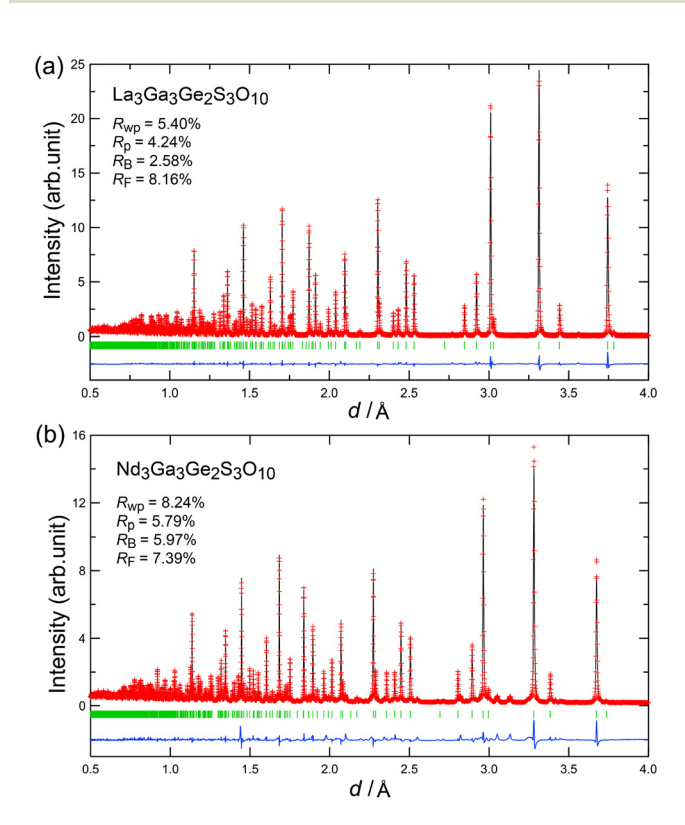


Fig. 5 Neutron powder diffraction patterns collected from (a)  $La_3Ga_3Ge_2S_3O_{10}$  and (b)  $Nd_3Ga_3Ge_2S_3O_{10}$  at room temperature. Rietveld refinements were performed on the basis of the structural models determined by single crystal structure analysis.

Munk function. The optical band gaps of Ln = La, Ce, Pr, and Nd estimated by the extrapolation method were 4.70, 3.51, 4.60, and 4.64 eV, respectively. Similar band gap values for Ln = La, Pr, and Nd are consistent with the similar Ln 5d energy levels.<sup>25</sup>

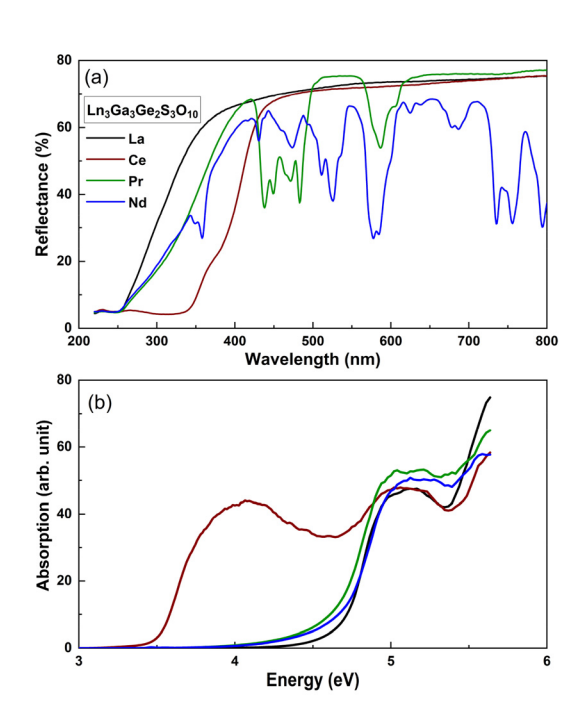


Fig. 6 (a) UV-Vis–NIR diffuse reflectance and (b) absorption spectra of  $Ln_3Ga_3Ge_2S_3O_{10}$  (Ln = La, Ce, Pr, Nd). The bandgaps were estimated to be 4.70, 3.51, 4.60, and 4.64 eV, respectively.

### SHG measurements

The powder SHG intensities of Ln<sub>3</sub>Ga<sub>3</sub>Ge<sub>2</sub>S<sub>3</sub>O<sub>10</sub> (Ln = Ce, Pr) were measured using the Kurtz–Perry method at  $\lambda$  = 1064 nm, with polycrystalline KDP as a reference compound. The SHG signals are plotted as a function of particle size in Fig. 7. The SHG intensities of both phases increased with increasing particle size in the size region smaller than 150  $\mu$ m, and were almost saturated in the larger particle size region. These behaviors indicate that they are type-I phase-matchable like



**Dalton Transactions** Paper

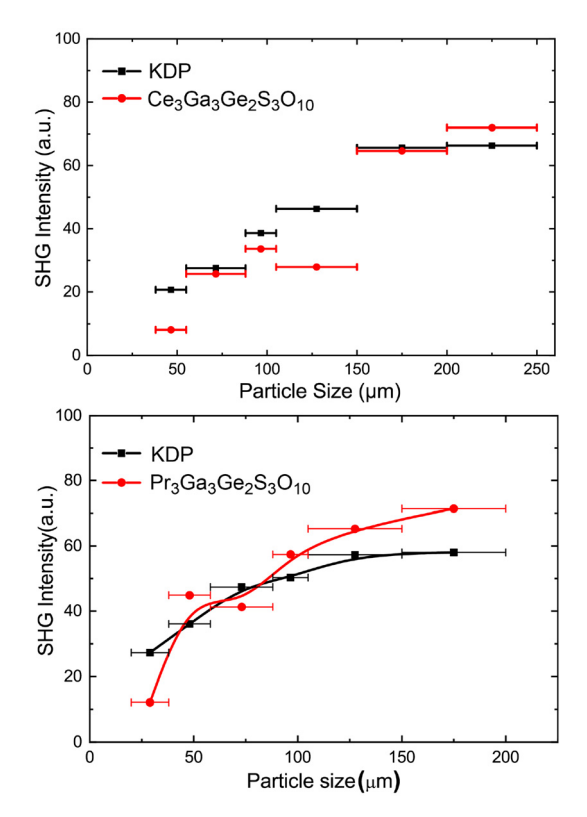


Fig. 7 Plots of SHG intensity vs. particle size at 1064 nm for  $Ln_3Ga_3Ge_2S_3O_{10}$  (Ln = Ce, Pr) and the reference compound  $KH_2PO_4$ (KDP). Solid lines are drawn as guides to the eyes.

La<sub>3</sub>Ga<sub>3</sub>Ge<sub>2</sub>S<sub>3</sub>O<sub>10</sub> and Nd<sub>3</sub>Ga<sub>3</sub>Ge<sub>2</sub>S<sub>3</sub>O<sub>10</sub>. 8,12 The SHG intensities of Ln = Ce and Pr are comparable to that of KDP at the largest particle sizes measured, but somewhat smaller than those of the La and Nd analogs ( $\sim$ 2 × KDP). These high SHG intensities are consistent with a previous theoretical conclusion that the Ga/Ge-centered tetrahedra forming non-centrosymmetric sublattices are mainly responsible for the SHG response of  $La_{3}Ga_{3}Ge_{2}S_{3}O_{10}$ .  $^{8,26,27}$ 

## Conclusions

Although a Ga/Ge disordered state was previously suggested for single crystals of La<sub>3</sub>Ga<sub>3</sub>Ge<sub>2</sub>S<sub>3</sub>O<sub>10</sub>, re-investigation by single-crystal XRD and neutron diffraction experiments performed in this study showed that La<sub>3</sub>Ga<sub>3</sub>Ge<sub>2</sub>S<sub>3</sub>O<sub>10</sub> has a Ga/Ge ordered state. Similar cation-ordered arrangements were observed for other lanthanide analogues. UV-Vis-NIR absorption spectra revealed band gaps larger than 4.60 eV for  $La_{3}Ga_{3}Ge_{2}S_{3}O_{10}$ ,  $Pr_{3}Ga_{3}Ge_{2}S_{3}O_{10}$ , and  $Nd_{3}Ga_{3}Ge_{2}S_{3}O_{10}$ , except for Ce<sub>3</sub>Ga<sub>3</sub>Ge<sub>2</sub>S<sub>3</sub>O<sub>10</sub> with a small band gap value of 3.51 eV because of Ce-4f<sup>1</sup> electronic configuration.

## Conflicts of interest

The authors declare no competing financial interests.

# Data availability

The data supporting this article have been included as part of ESI. X-ray crystallographic files for the structure have been deposited in Cambridge Crystallographic Data Centre (CCDC) with no. of 2449159, 2449160, 2449238, and 2449239.†

# Acknowledgements

This study was supported by World Premier International Research Center Initiative (WPI), the Japan Society for the Promotion of Science (JSPS) KAKENHI (grant no. 25K01507, 25K01657. 25H01652), Bilateral Program (No. JPJSBP120237714), and Core-to-Core Program (JPJSCCA20200004). Y. T. acknowledges the grant from the Murata Science Foundation. We also acknowledge Dr Ishigaki for his assistance in the NPD experiments with iMATERIA with the approval of J-PARC (Proposal No. 2023PM2001, 2024PM2001, 2025PM2002) and Prof. Z. Yang and Prof. S. Pan from Xinjiang Technical Institute of Physics and Chemistry, CAS for the SHG measurements.

## References

- 1 H. Kageyama, K. Hayashi, K. Maeda, J. P. Attfield, Z. Hiroi, J. M. Rondinelli and K. R. Poeppelmeier, Nat. Commun., 2018, 9, 772.
- 2 M. Orr, G. R. Hebberd, E. E. McCabe and R. T. Macaluso, ACS Omega, 2022, 7, 8209-8218.
- 3 J. Huang, S. Shu and G.-M. Cai, Cryst. Growth Des., 2022, 22, 1500-1514.
- 4 Y. Zhang, H. Wu, Z. Hu and H. Yu, Chem. Eur. J., 2023, 29, e202203597.
- 5 B. W. Liu, X. M. Jiang, G. E. Wang, H. Y. Zeng, M. J. Zhang, S. F. Li, W. H. Guo and G. C. Guo, Chem. Mater., 2015, 27, 8189-8192.
- 6 Y. Tsujimoto, C. Juillerat, W. Zhang, K. Fujii, M. Yashima, P. S. Halasyamani and H.-C. zur Loye, Chem. Mater., 2018, 30, 6486-6493.
- 7 J. jing Xu and K. Wu, Coord. Chem. Rev., 2023, 486, 215139.
- 8 H. Yan, Y. Matsushita, K. Yamaura and Y. Tsujimoto, Angew. Chem., Int. Ed., 2021, 60, 26561-26565.
- 9 B. Zhang, G. Shi, Z. Yang, F. Zhang and S. Pan, Angew. Chem., Int. Ed., 2017, 56, 3916-3919.
- 10 G. Shi, Y. Wang, F. Zhang, B. Zhang, Z. Yang, X. Hou, S. Pan and K. R. Poeppelmeier, J. Am. Chem. Soc., 2017, 139, 10645-10648.
- 11 H. Liu, Z. Song, H. Wu, Z. Hu, J. Wang, Y. Wu and H. Yu, ACS Mater. Lett., 2022, 4, 1593-1598.
- 12 M. Y. Ran, S. H. Zhou, W. B. Wei, B. X. Li, X. T. Wu, H. Lin and Q. L. Zhu, Small, 2023, 19, 2300248.
- 13 M. S. Zhang, S. M. Pei, X. M. Jiang, B. W. Liu and G. C. Guo, ACS Mater. Lett., 2024, 3, 312-318.

**Paper** 

14 A. P. Dudka and B. V. Mill', *Crystallogr. Rep.*, 2013, **58**, 594–603.

- 15 L. A. Gorelova, V. A. Yukhno, M. G. Krzhizhanovskaya and O. S. Vereshchagin, *J. Solid State Chem.*, 2024, **329**, 124429.
- 16 H. Bazzaoui, C. Genevois, D. Massiot, V. Sarou-Kanian, E. Veron, S. Chenu, P. Beran, M. J. Pitcher and M. Allix, *Inorg. Chem.*, 2022, 61, 9339–9351.
- 17 G. M. Sheldrick, Acta Crystallogr., Sect. A:Found. Adv., 2015, 71, 3-8.
- 18 G. M. Sheldrick, Acta Crystallogr., Sect. C:Struct. Chem., 2015, 71, 3-8.
- 19 O. V. Dolomanov, A. J. Blake, N. R. Champness and M. Schröder, *J. Appl. Crystallogr.*, 2003, 36, 1283–1284.
- 20 T. Ishigaki, A. Hoshikawa, M. Yonemura, T. Morishima, T. Kamiyama, R. Oishi, K. Aizawa, T. Sakuma, Y. Tomota,

- M. Arai, M. Hayashi, K. Ebata, Y. Takano, K. Komatsuzaki, H. Asano, Y. Takano and T. Kasao, *Nucl. Instrum. Methods Phys. Res.*, *Sect. A*, 2009, **600**, 189–191.
- 21 R. Oishi, M. Yonemura, Y. Nishimaki, S. Torii, A. Hoshikawa, T. Ishigaki, T. Morishima, K. Mori and T. Kamiyama, *Methods Phys. Res., Sect. A*, 2009, 600, 94–96.
- 22 R. D. Shannon, Acta Crystallogr., Sect. A, 1976, 32, 751-767.
- 23 N. E. Brese and M. O'Keeffe, *Acta Crystallogr., Sect. B:Struct. Sci.*, 1991, 47, 192–197.
- 24 W. H. Baur, Acta Crystallogr., Sect. B, 1974, 30, 1195-1215.
- 25 Y. Shimizu and K. Ueda, J. Lumin., 2015, 168, 14-19.
- 26 B.-H. Lei, S. Pan, Z. Yang, C. Cao and D. J. Singh, *Phys. Rev. Lett.*, 2020, 125, 187402.
- 27 Z. Yang and S. Pan, Chin. Sci. Bull., 2024, 69, 4197-4208.